JET–P(97)35

The Use of Atomic and Molecular Data in Fusion Plasma Diagnostics

H P Summers[1], H Anderson[1], N R Badnell[1], F Bliek[2], D C Griffin[3], M von Hellermann, R Hoekstra[2], A Howman, L D Horton, R Konig, G M McCracken, C F Maggi, M G O'Mullane[1], M S Pindzola[5], R E Olson[4] and M F Stamp

JET Joint Undertaking, Abingdon, Oxfordshire, OX14 3EA,
[1]Department of Physics and Applied Physics, University of Strathclyde, Glasgow G4 0NG UK.
[2]Kernversneller Instituut, Zernikelaan 100, AA-Groningen, Netherlands.
[3]Department of Physics, Rollins College, Winter Park, Florida 32789 USA.
[4]Department of Physics, University of Missouri, Rolla, Missouri 65401 USA.
[5]Department of Physics, Auburn University, Auburn, Alabama 36849 USA.

October 1997

The use of atomic and molecular data in fusion plasma diagnostics

H P Summers†, H Anderson†, N R Badnell†, F W Bliek§, D C Griffin♭, M von Hellermann‡ , R Hoekstra§, A Howman‡ , L D Horton‡ , R Konig‡ , G M McCracken‡ , C F Maggi‡ , M G O'Mullane† , M S Pindzola♮, R E Olson♯ and M F Stamp‡

† *Department of Physics and Applied Physics, University of Strathclyde, Glasgow G4 0NG, UK*

‡ *JET Joint Undertaking, Abingdon, Oxon. OX14 3EA, UK*

§ *KVI, Atomic Physics, Zernikelaan 25, 9747 AA Groningen , Netherlands*

♭ *Department of Physics, Rollins College, Winter Park, Florida 32789, USA*

♯ *Department of Physics, University of Missouri, Rolla, Missouri 65401, USA*

♮ *Department of Physics, Auburn University,Auburn, Alabama 36849, USA*

Abstract.

Considerable attention in modern large fusion experiments is focused on neutral beam penetrated plasma and on divertor plasma. In the former, ion/atom reactions drive the population dynamics while in the latter, although electron processes predominate, there are significant ion/atom and atom/atom influences. Neutral atoms in beams, impurities in beam penetrated plasma and complex partially ionised impurities in divertor plasma find themselves in the collisional radiative regime where the simple stationary excitation/cascade picture of the coronal model is invalidated by secondary collisions. Thus atomic data needed in such fusion applications are not a few reaction cross-sections but large complete sets which support full collisional-radiative models. Also, experiment analysis does not make use directly of fundamental atomic data but rather effective coefficients deduced from such models.

In the paper, we describe two cases. The first is neutral deuterium beam attenuation and beam emission and its linking to active diagnostic spectroscopy using beams. We describe how the diagnostic analysis and experimental data reduction are carried out efficiently using derived effective stopping and effective emission coefficients. Then we describe the organisation of the fundamental ion/atom data and how collisional-radiative modelling generates the effective coefficients from them. This is an area in which long-term, intensive collaborative effort on both the fundamental data and the detailed spectral reduction is now bearing fruit. The second case is the more general task of modelling ionisation state, power and impurity line emission for interpretation of divertor observations. We explain the matching of effective collisional-radiative coefficients to the diver-

tor plasma models and of photon emission coefficients to the post-processing for particular spectrometers and lines-of-sight. Then, we illustrate how just one part of the substantial fundamental atomic data requirement - dielectronic recombination - must be prepared for the application. Finally, the generalised collisional-radiative model, which prepares the effective coefficients, is described and we explain how it gives proper attention to the dynamic nature and non-negligible density of the divertor plasma and why resolution of metastable states is a requirement. The Atomic Data and Analysis Structure, ADAS and the JET Joint Undertaking Experiment are used in illustration.

I INTRODUCTION

This paper is concerned with how atomic and molecular data are used in fusion research. Rather than attempting an exhaustive review of applications we have chosen to focus on just two important areas. These are (a) charge exchange / beam emission spectroscopy with neutral deuterium beams and (b) modelling / spectral diagnosis of divertor plasma. Both are of very considerable interest at the present time and are expected to remain so into the future. Also, both use large quantities of atomic data and this use is quite well developed. Thus the problems of access to data, its general management and its provision at the point of diagnostic or modelling need in appropriate forms have been examined and solved. They will also illustrate a secondary theme of the paper, namely, that they are derived atomic/molecular data produced by reaction kinetic (collisional-radiative) models in plasmas rather than fundamental data which are actually used in application. Such models use and maneouver so much fundamental data that the latter must be carefully structured and organised from the beginning.

As is well known, the introduction of neutral deuterium heating in fusion plasmas initiated a complete new approach to the spectroscopy of the core plasma. This followed because electron transfer from the deuterium beam atoms to bare nuclei in the plasma core allowed the latter to radiate. Since such 'charge transfer' is generally to excited states, consequential spectral line radiation is observable in the visible. Quantitative study of this radiation requires knowledge of the local neutral deuterium beam atom density in the viewed volume. This can be deduced in principle provided the beam particle energies and fluxes are known at the point where the beam enters the plasma and the beam attenuation process can be modelled. A number of the key attenuation reaction processes have been measured and very large efforts have been made over the last decade to expand and improve the theoretical data collection so that the effects of all light impurities likely to be present in the plasma can be included. Nonetheless the demand of quality on such data is very high since analysis using calculated attenuation to the observed volume strongly amplifies the influence of error in the fundamental reactions [14]. The more recent observations of the emission by excited deuterium in the

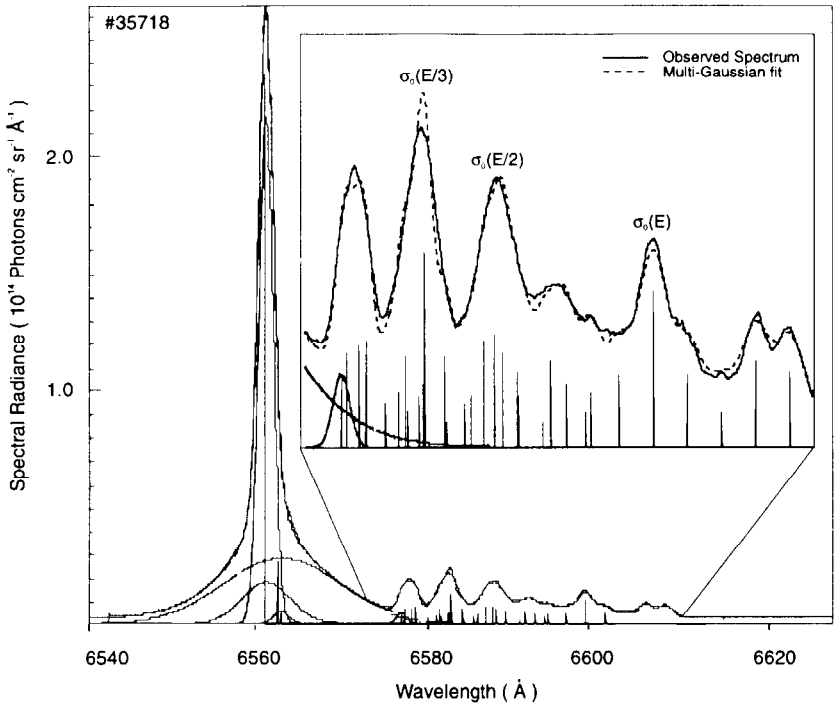

FIGURE 1. Observed motional Stark D_α spectral feature. The emission feature was recorded during the JET pulse 35718 using track 4 of the multichord visible spectroscopy system. The tangential bank was active with a primary energy of 140keV. (cf. von Hellermann (1993) [9] for a specification of the geometry). The constrained multigaussian spectral fit to the interval is also shown. Particular attention should be brought to the annotation of the full, half and one-third σ_0 Stark components. Due to the existence of three fractional energy components in the beam this gives rise to three Stark multiplets. Each Stark multiplet is Doppler shifted according to the velocity of the relevant beam neutrals and as a result the overal picture is an overlap of each Stark feature. A somewhat more complicated situation arises when the radial bank is also on as this results in the overlap of 6 Stark multiplets.

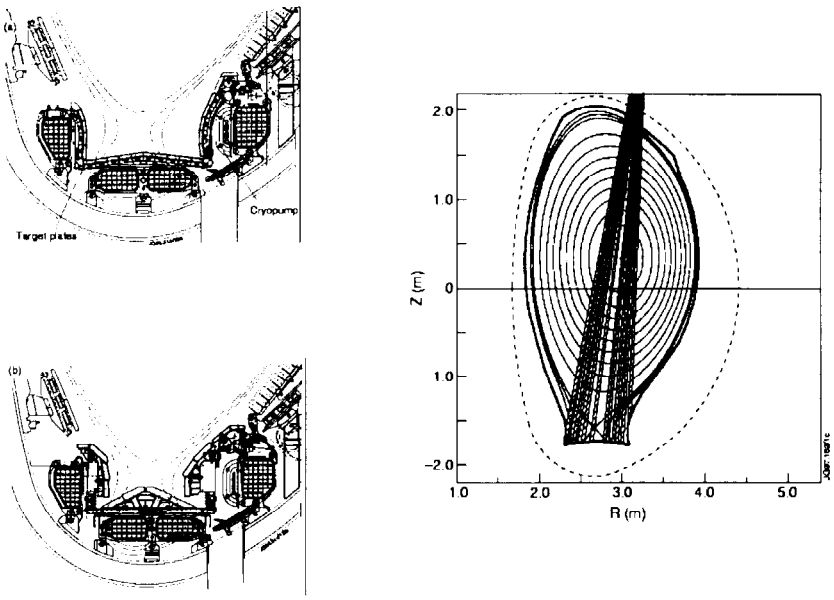

FIGURE 2. (a) Schematic poloidal section of the JET torus showing the geometrical arrangement of the coils and target plates of the JET Mk1 divertor. (b) Schematic of the Mk2A divertor. (c) Typical reconstructed poloidal section of the magnetic flux surfaces showing the last closed flux surface and the strike zones of the scrape-off-layer plasma with the target plates. Viewing lines used for visible spectroscopic studies are superimposed for illustration.

beams themselves [4] introduced a powerful new spectral diagnostic built on the subtlety of the motional Stark distortion of the D_α emission feature and the substantial Doppler shifts of the features in oblique viewing lines. It also promised an improvement over the beam attenuation calculation for the local neutral density since the density could instead be deduced directly from the localised D_α intensity. In practice, this has proved difficult to achieve for several reasons. The basic observed beam emission feature is a Doppler shifted D_α motional Stark multiplet. The observed D_α Stark multiplet is in fact a superposition of such features from different injectors and from different energy fractions within each individual injector. The appearance of the 6540Å - 6620Å spectral interval is shown in figure 1. Such observations together with visible charge exchange spectroscopic signals from impurities allow the local deposition of beam energy and particles, local impurity densities and related parameters to be deduced and this must be done self-consistently. At JET Joint Undertaking, the matching of the various observations and their merging with additional JET diagnostic signals, including radial profiles of electron temperature and density, are conducted iteratively in a complex experimental analysis package called CHEAP ('CHarge Exchange Analysis Package') [9].

Current thinking on control of the interaction of the particle and energy

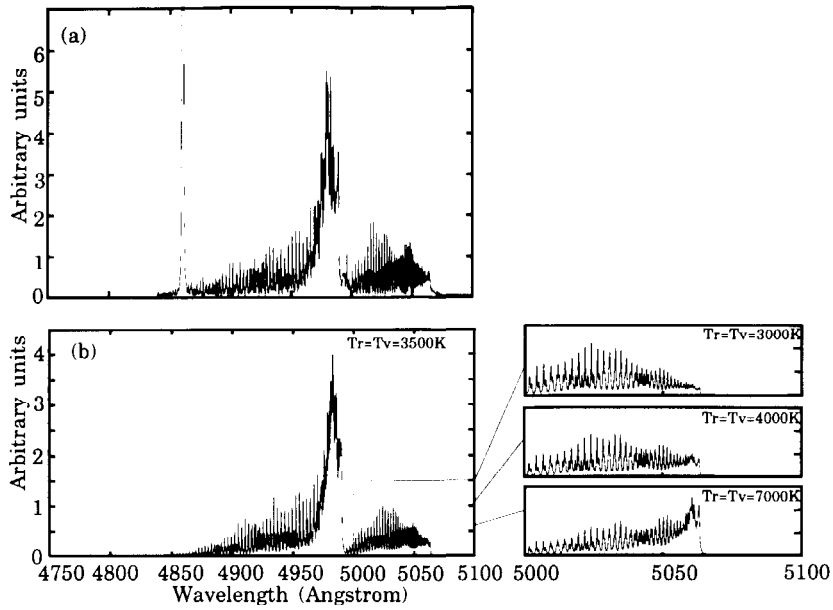

FIGURE 3. (a) Observed spectrum of the 4850-5100Å region (JET Pulse #35687 at 14.5s) showing BeD ($A\ ^2\Pi - X\ ^2\Sigma$). (b) Simulated 0-0, 1-1 and 2-2 bands at T_r=3500K and T_v = 3500K. The insert shows the variation of the P branch with temperature. [7]

flux flowing from the fusion plasma with material surfaces indicates that a cool divertor region remote from the main plasma is a necessary part of fusion reactor design. Over the last eight years implementation of the axi-symmetric poloidal divertor concept on the JET machine has led to extensive redesigning of the vessel interior and magnetic field coils to produce appropriate magnetic null (X-point) positions, connection lengths and divertor target tiles for the plasma flowing down the scrape-off-layer. Experimental campaigns have investigated the properties of the Mk1 and Mk2A designs. The next stage in this evolution is the Mk2GB (gas box) design due for installation at the end of 1997. Many diagnostic systems were upgraded and optimised prior to plasma operation with the Mk1 divertor [5]. As a result of the improved divertor spectroscopy the MK1 divertor campaign has given the opportunity for detailed sets of observations of impurity atoms and ions and in some cases their molecular precursors in JET. Spectral observations of the divertor are rich. Figure 3 of a visible wavelength segment and figure 4 in the VUV show some examples. The geometrical complexity of the divertor plasma region, the open magnetic field line structure, the localisation of power deposition flowing in the scrape-off-layer at the strike zones and divertor operational strategies such as the creation of detached radiating plasma present a diagnostic challenge. The divertor plasma is neither homogeneous nor stationary as the time

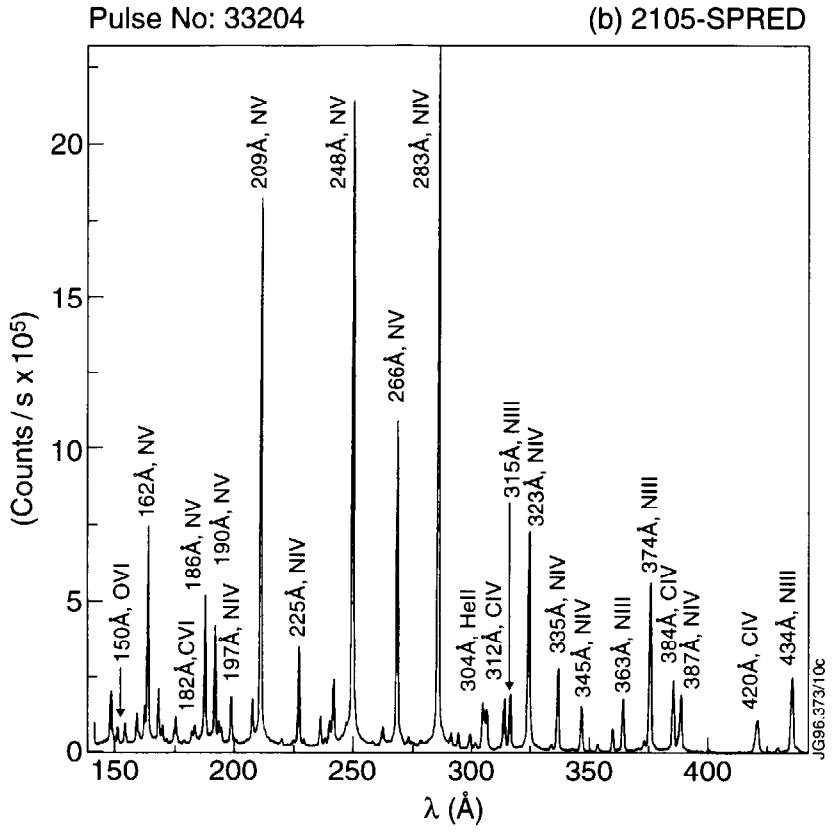

FIGURE 4. VUV spectra of the divertor from the 2105-SPRED during a nitrogen seeded radiative divertor discharge (Pulse 33204) [11]

constants for parallel movement of low ionisation stages of impurities from the strike zones and for high stages of ionisation from the bulk plasma into the divertor can be comparable to ionisation and recombination times. Thus the usual equilibrium ionisation vehicle for spectral interpretation is not sustainable. Instead, it is necessary to link the spectral observations, dynamic divertor plasma models and the atomic modelling of the radiating plasma closely from the beginning. Multiple probes along the divertor target, tomographic bolometric reconstructions together with comprehensive wavelength spectroscopy along multiple lines of sight through the divertor provide the experimental pulse data. Such signals are simulated in an interconnected set of modelling and post-processing steps and then the simulations and experiments compared.

In its approach to the study of these two areas, JET is fairly typical of other fusion experiments such as ASDEX-upgrade, ALCATOR-Cmod, JT60 and DIIID.

II THE ATOMIC DATA AND ANALYSIS STRUCTURE, ADAS

At JET Joint Undertaking, we took the view that atomic data should be a responsibility of the experimental, spectroscopy division (Experimental Division II) since it was there that the most testing use and scrutiny would take place. A tightly defined, integrated computational approach was taken to the provision of appropriate derived atomic data for diagnosis and modelling. This is known as the Atomic Data and Analysis Structure, ADAS. Several fusion laboratories have worked with JET in the shared development of ADAS into its present guise as a UNIX workstation code and data package. In the discussion of beam and divertor atomic physics data and modelling, we shall from time to time refer to ADAS [15]. ADAS data, both fundamental and derived, are currently assigned to one of twenty-six data format classes, called *adf's*, such as *adf*01 and *adf*02. ADAS codes are allocated to six series each containing about ten codes. Thus the ninth code of series 2 is called ADAS209. In the schematics of data and program flows of the later parts of the paper, we use these names when we have an ADAS implementation.

III DEUTERIUM BEAM STOPPING, BEAM EMISSION AND CHARGE EXCHANGE SPECTROSCOPY

Deuterium atoms in beams penetrate the confining magnetic field of the plasma as neutrals until their point of ionisation. The rate of beam energy deposition at any point along the beam path is obtained therefore from the

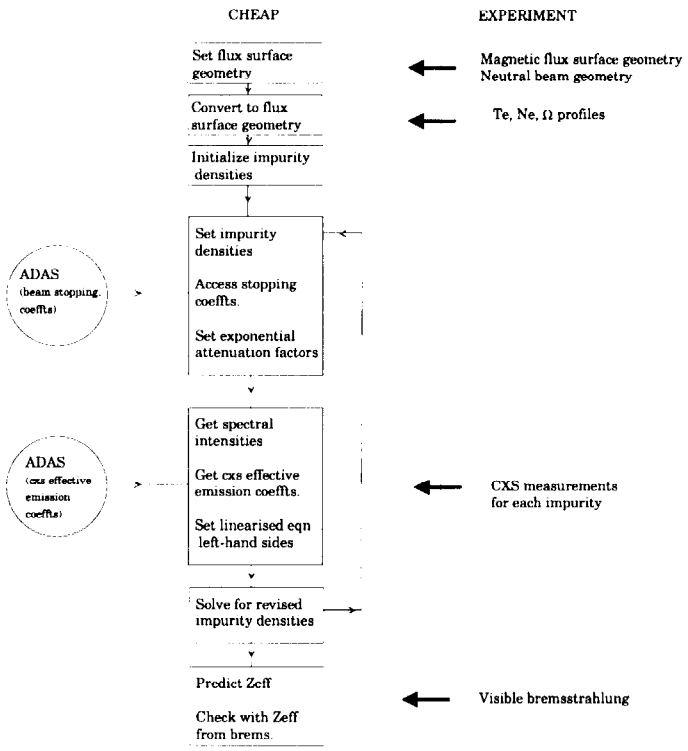

FIGURE 5. Organisation of the CHEAP analysis showing the entry points of derived atomic data

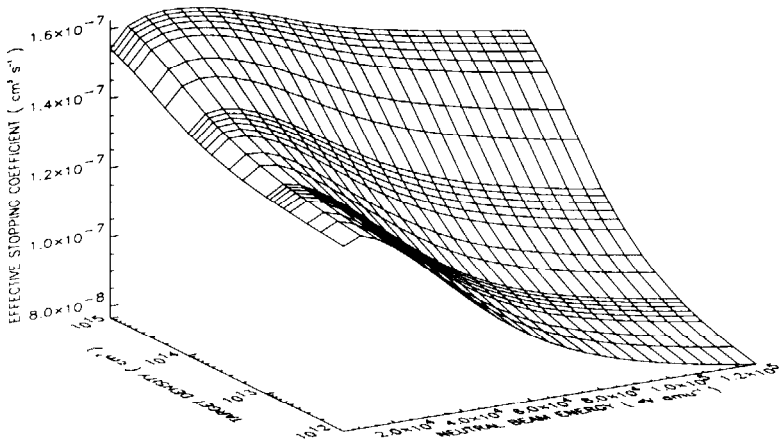

FIGURE 6. Variation of the effective deuterium beam stopping coefficient with beam energy and electron density. Pure deuterium plasma at $T_i = 2.0 * 10^3$ eV.

ionisation rate, R, or from the effective ionisation rate coefficient, $S_B^{(e)}$ with $R = N_e N_{D,beam} S_B^{(e)}$ if the electron density N_e is known. $S_B^{(e)}$ is usually known as the stopping coefficient. The neutral deuterium density in the beam , $N_{D,beam}$ at any point of the beam path can be obtained by using $N_e S_B^{(e)}$ to calculate the attenuation from where the beam enters the plasma. $S_B^{(e)}$ is written with reference to the electron density in the plasma, but it is primarily collisions with thermal deuteron and thermal impurity ions (fully ionised) which cause the ionisation. So $S_B^{(e)}$ depends on the impurity concentrations. Unfortunately, the concentrations, N_{D+}/N_e, and $\{N_{Z_i}/N_e : i = 1, ...\}$ in the plasma are not initially known except in so far as their mean Z_{eff} can be inferred from bremsstrahlung measurements. However, a part of the ionisation of the beam atoms takes place via a charge transfer reaction to the impurity ions in the plasma which then emit measurable spectral line radiation. Thus, the charge exchange spectroscopic line-of-sight intensity of radiation, $I_{Z_i,n\to n'}$ in a spectrum line $n \to n'$, which is localised at the intersection of the beam/ spectrometer viewing line intersection,L, may be used to infer N_{Z_i}, from $I_{Z_i,n\to n'} = \int_L N_{D,beam} N_{Z_i} q_{Z_i,n\to n'} dl$, if the effective emission coefficient $q_{Z_i,n\to n'}$ is known. We are therefore led to a circular iterative analysis based on plasma measurements and spectroscopy. At JET, the implementation is called 'CHEAP' and a schematic is shown in figure 5.

A The derived data

The beam stopping coefficient depends on density. This is because there

are stepwise losses through excited states of the beam deuterium atoms at fusion plasma densities. At the precision required of beam stopping coefficients for calculating attenuation to the centre of the plasma ($\leq 10\%$) such effects matter. Thus the beam stopping coefficient is an effective coefficient including the influence of the excited states. It is properly called a collisional-radiative coefficient. The behaviour of the coefficient is shown in figure 6. The secondary collisions which cause this step-wise ionisation are principally due to ion collisions (deuterons and impurity nuclei) and so the effective stopping coefficient is *itself* a function of the impurity concentrations. The *ab initio* re-evaluation of the stopping coefficient for varying impurity mixtures in the iterative CHEAP analysis is quite impractical. At JET we have evaluated the beam stopping for pure impurity plasmas, that is with only a single impurity and with the electron number density being that which comes from charge balance. Then a linear combination of coefficients for a mixed impurity plasma can be produced. The error of this step is assessed by comparison with exact calculation for a mixed plasma [1]. The error is below (5%). Thus a tabulation of the derived stopping coefficient is made for every light impurity $H, He, Li, Be, B, C, N, O, F$ and Ne. The effective coefficients are also functions of T_i, N_i and E_{beam}. The rapid extraction of the stopping coefficient from tabulations, required for inter-pulse analysis, does not permit interpolation through a multi-dimensional grid. The primary dependence of the stopping coefficient is on beam energy and ion density. We define reference conditions for the plasma parameters and beam energy relevant to JET and establish the stopping coefficient at a two-dimensional grid in E_{beam}/N_i at the reference condition of T_i. Then a one-dimensional scan in T_i is made at the reference values of E_{beam} and N_i. Such a mixed two- and one-dimensional scan structure of the tabulations delivers the required precision in the final interpolated coefficient and the required look-up speed. The prescribed structure follows ADAS format *adf*21. Revision of *adf*21 data takes place at intervals when there are improvements of the fundamental database from which it is built. The most recent reprocessing was carried out in June 1997 and made available through the ADAS network.

Charge exchange spectroscopy and beam deposition studies in the current CHEAP analysis calculate the attenuation of the beam from the point of entry to find the local neutral beam density at points along the beam line. The exponential attenuation causes a corresponding increase in the error bounds of this local density arising from the error in the stopping coefficient. Since the beam emission is observable (cf. figure 1) it might be thought that the local neutral density would be best deduced from this local observation. Such a deduction requires knowledge of the theoretical effective emission coefficient for Balmer alpha emission. The influences on this coefficient are the same as for the beam stopping coefficient with emphasis on losses from excited states of the beam deuterium atoms. Figure 7 shows the behaviour of the effective beam emission coefficient. The two methods of deduction have historically

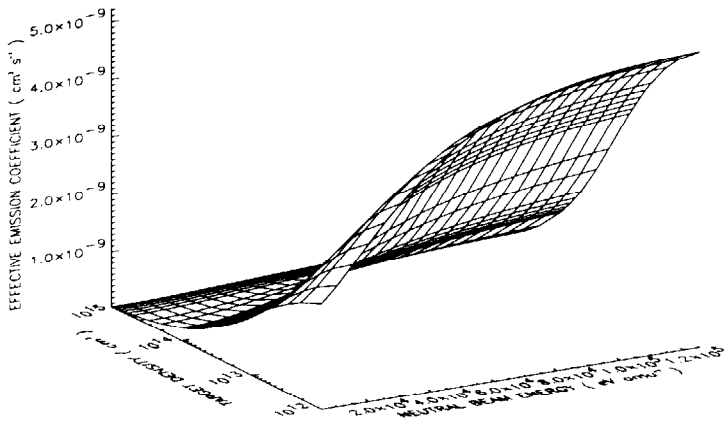

FIGURE 7. Variation of the effective Balmer alpha beam emission coefficient with beam energy and electron density. Pure deuterium plasma at $T_i = 2.0 * 10^3$ eV.

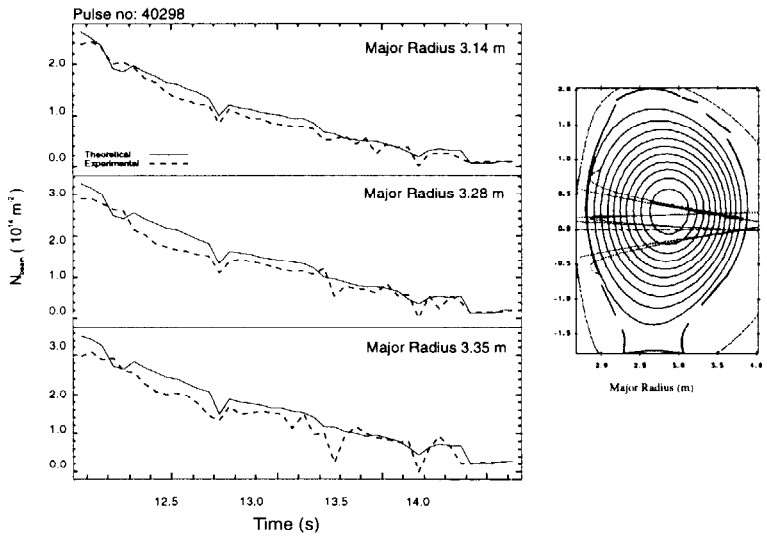

FIGURE 8. Time evolution of the line-integrated neutral beam density at three different radial positions. The solid curve is the line integral neutral deuterium number density from the attenuation calculation. The dashed curve is the line integral number density obtained from the measured Balmer alpha intensity. The latter also uses the collisional-radiative model to convert from excited population to ground population. The insert shows the paths of the individual contributing beam lines in flux surface geometry.

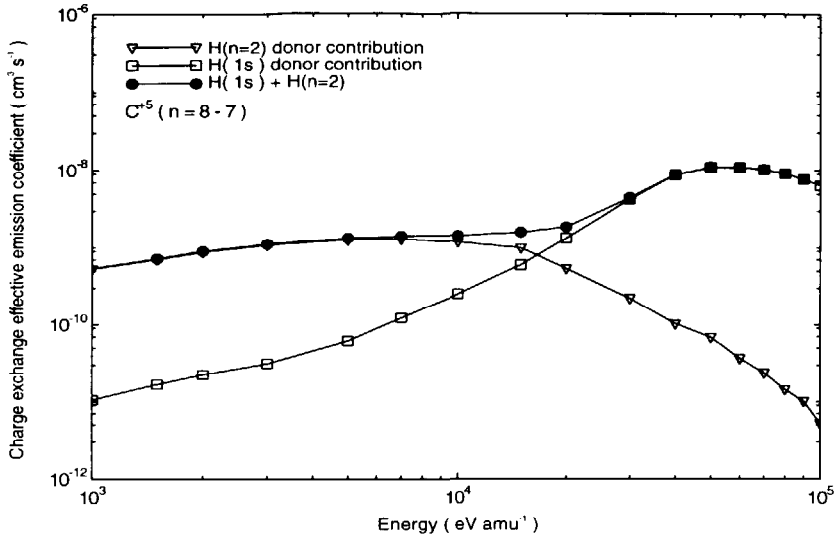

FIGURE 9. Behaviour of the charge exchange effective emission coefficient for the $n = 8 - 7$ line of CVI. $Z_{eff} = 2, T_i = 8.0 * 10^3$eV, $N_i = 5.0 * 10^{13}$cm^{-3}

given results which differed typically by up to factors of three. This situation now seems to have been corrected. We have conducted a detailed review of the fundamental atomic data, error analysis of the derived coefficients, step by step validation of experimental spectroscopic, beam and plasma data entry and flow through CHEAP and detailed examination of our fitting of the motional Stark split observed feature. The various improvements now yield an accuracy and consistency of $\sim$ 20%. Present results are shown in figure 8. We now believe the beam emission can be used in the manner originally envisaged. It is to be noted that the structure used for access and storage of beam stopping coefficients are immediately usable again for beam emission. We use an identical ADAS data organisation but called *adf*22 rather than *adf*21.

The improved precision in our knowledge of the excited populations in the beam allows progress in charge exchange spectroscopy. For relatively fast beams ($\sim$ 70keV/amu) with modest fractional energy components, charge exchange spectroscopy in the visible spectral region is dominated by donation from the ground state of the deuterium beam atom. This stuation changes as we move to lower energies where donation from excited states matters. We have improved the state selective charge exchange database for donation from $D(n = 2)$ to light impurity nuclei [3]. These new data are now being combined with the beam population results to provide a low beam energy correction to the charge exchange effective emission coefficients. Figure 9 illustrates the role of the excited beam donor in the CVI (n=8-7) line emission.

B The fundamental data

The derived collisional-radiative effective beam coefficients used and described above depend on high quality collision-cross-section data for positive ion/hydrogen reactions. These include ionisation, charge transfer and excitation reactions with all fully ionised light impurity nucei from hydrogen to neon. Electron impact cross-sections for ionisation and excitation are also needed. The effective coefficients for charge exchange spectroscopy of plasma impurities in turn require very large collections of state selective charge exchange cross-sections for neutral hydrogen (ground and excited state) with fully stripped light impurity ions. These data are required over extended energy ranges and resolved to the nl levels of the receiver. Considerable effort has been put into creating and assembling such data over the years. There are some substantial new additions. These are described in the accompanying paper by Hoekstra [10].

C Collisional-radiative modelling and the computational implementation

We have found it advantageous to embed the calculation of beam stopping and beam emission for hydrogen in a more general picture of neutral hydrogen as a radiating, ionising and recombining species in the fusion plasma. This is because an initial fast neutral beam hydrogen atom can lead to a high temperature thermal hydrogen atom in a beam halo and ultimately to a lower temperature thermal hydrogen atom at the plasma periphery. Also with the variation of primary beam energies which occur in fusion experiments (40 keV/amu - 70 keV/amu typically for deuterium) and the inevitable fractional energy components (35 keV/amu and 23 keV/amu for the JET primary 70 keV/amu beams) there is a wide range of energies of hydrogen donors present which influence observed charge exchange impurity spectra and contribute to the overall composite $D\alpha$ feature. For fast beams, ground state donors primarily drive the visible impurity charge exchange spectra while at thermal energies it is almost entirely excited donors which do this. From the point of view of the hydrogen atom populations, the most important type of collision alters also from being ion impact at beam energies to electron impact in the lower temperature thermal regimes. In the thermal regime, recombination of hydrogen nuclei by both free electron capture and charge exchange capture balances ionisation while in the beams, the hydrogen atom is strictly ionising and a charge exchange donor. From this viewpoint, the beam atom is distinguished simply as one with a high fixed translational velocity which enters into the collisionality together possibly with enhanced state mixing from a motional Stark electric field. Because of the strong l-shell mixing, we work in the bundle-n picture. Consistent modelling of the type sought here should

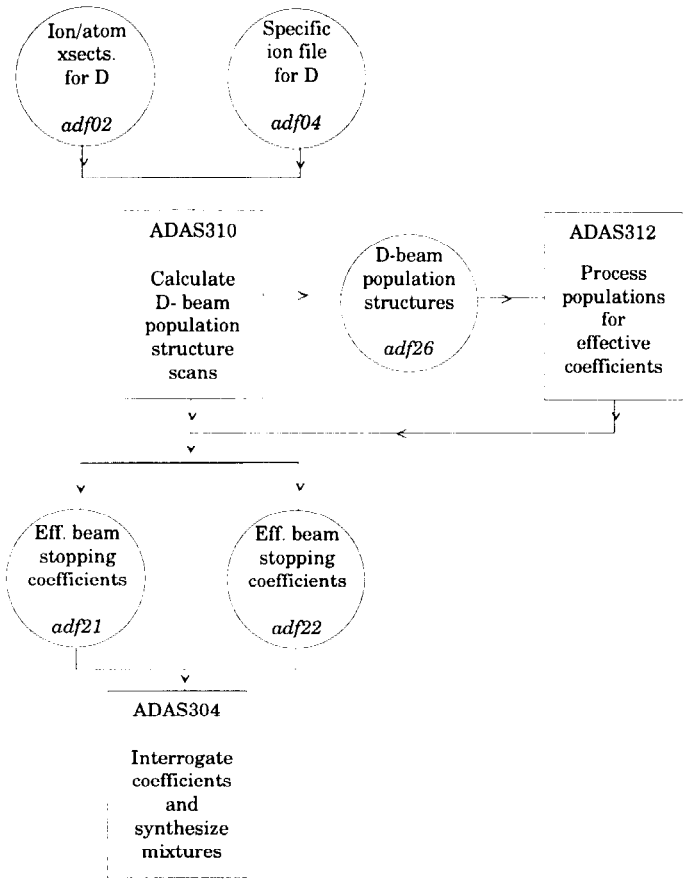

FIGURE 10. Schematic of ADAS codes and data sets used in neutral deuterium beam studies. There is an equivalent schematic for charge exchange spectroscopy with deuterium beams which is not shown here.

work smoothly between these different regimes and use the same fundamental data. It is not a difficult task to generalise computationally in this manner and it has the added merit of allowing stringent testing of Saha-Boltzmann limits, zero-density ionising extremes etc.

Three ADAS codes and five data formats provide the computational and data archiving functionality for the beam analysis as shown in the schematic of figure 10. *adf*02 and *adf*04 are structured assemblies of fundamental reaction cross-sections and rates. *adf*21, *adf*22, and *adf*26 are derived data generated by the collisional radiative codes.

- ADAS304 - interrogates effective beam stopping and emission coefficients and assembles effective coefficients for impurity mixtures
- ADAS310 - calculates beam atom excited populations and stopping coefficients in the bundle-n approximation

- ADAS312 - post-processes population data from ADAS304 to assemble effective coefficient collections suited to rapid experiment analysis

IV MODELLING AND SPECTRAL DIAGNOSIS OF THE DIVERTOR

The highly ionising environment near the divertor strike zones, from the point of view of neutral and near neutral impurities emerging from the surfaces, has become familar in recent years. Atomic modellers calculate the derived 'ionisation per photon' coefficients for quick estimation of impurity fluxes in these circumstances [8]. However, the divertor also has recombining environments and it is found that the passage of ions through them and the power which they radiate there matters for the overall divertor power balance. Also, most observations have lines-of-sight which cross these different, usually geometrically complex regions. The 'experimental' approach at JET to diagnostic study of the divertor is that of modelling observed signals and then comparison with the actual observed signals [12]. Such an approach is almost mandatory for other than the simplest reductions of observed data. This has the disadvantage of requiring the use of the complete (or nearly complete) theoretical computational models of divertor fluid and particle transport (and their slow execution times) but with the advantage of allowing manipulation of relevant physical parameters in seeking the simulation/observational match. This means that derived collisional-radiative atomic data enters the picture both in the form of source terms for the fluid and particle transport codes and as effective emissivity and radiant power data for the post-processing of the modelled ion distributions into simulated line-of- sight signals. A schematic of the JET approach is shown in figure 11. The entry points, indicated in the figure as ADAS, show the derived atomic data needed for the JET plasma modelling and diagnosis. Such derivative data are the actual targets of fundamental atomic data creation and the subsequent atomic modelling.

A The derived data

Collisional-radiative theory allows us to identify the appropriate types of derived data needed for each impurity ion from a consideration of time constants. Slowly relaxing state populations are large and must enter the plasma dynamic equations explicitly. So for those we need effective recombination and ionisation coefficients and related power coefficients. Fast relaxing state populations are small and they reach a local quasi-static equilibrium with respect to the slowly relaxing populations. For those we need effective emission coefficients which relate emission in any line to the large populations. In certain situations in the divertor, the large populations include metastable as well as

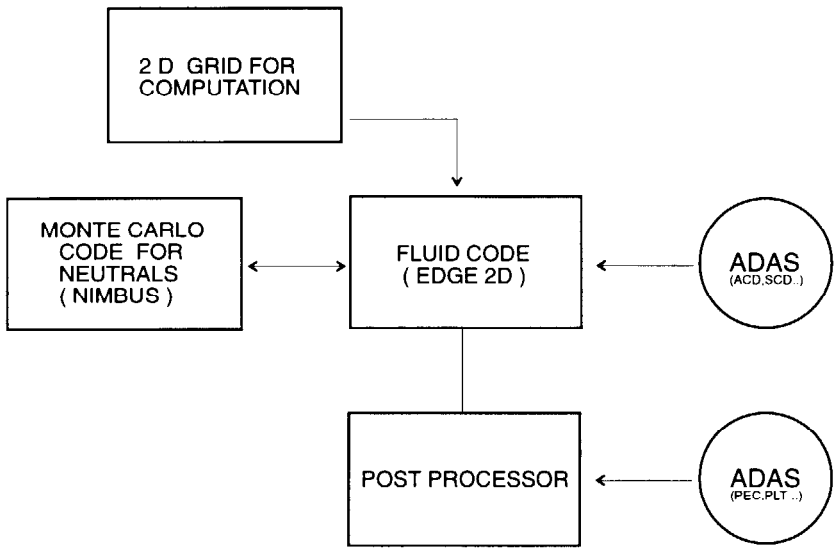

FIGURE 11. Schematic of the plasma modelling codes and post-processing used in simulating and analysing JET divertor signals. *2D grid*: from reconstruction of the magnetic equilibrium, generates a 2D field aligned net on which the computation is carried out. *Fluid code*: solve the 2D fluid equations for each species: electron, plasma and impurity ions (every charge state) are treated as species. *Monte Carlo code for neutrals*: particle, momentum, energy sources and losses for the plasma, neutral hydrogen isotope distributions, neutral impurity distributions. *Post − processor*: after the solution is obtained, performs integrations along diagnostic lines of sight of line emissivities, radiation profiles etc. *ADAS*: points of insertion of collisional-radiative atomic data.

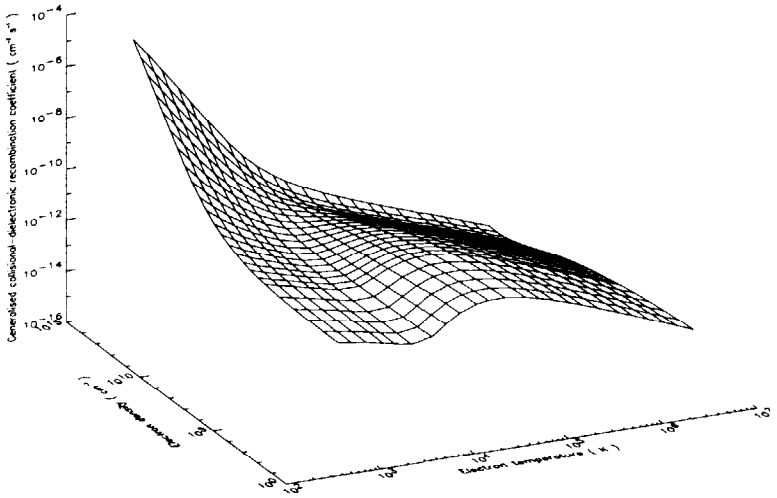

FIGURE 12. Generalised collisional-radiative recombination coefficient for $C^{+2}_{2s^2\ {}^1S} + e \rightarrow C^{+1}_{2s^2 2p\ {}^2P}$. This is the ground state to ground state part of the metastable resolved data. Note the high density three-body regime at low temperatures and the suppression of the high temperature dielectronic part at higher densities before three-body recombination takes over.

ground state populations. At JET and in ADAS, we have taken the approach that a complete set of metastables is the best starting collection of 'large' (usually called 'dynamic') populations [16]. Such a collection can be simplified (by grouping) in less dynamic regions or kept separate in more dynamic regions. In fusion plasma modelling, it is unnecessary to treat excited state populations as dynamic. We use the terms 'generalised collisional-radiative modelling' and 'metastable resolved treatment' when we distinguish metastables. Metastable resolution provides a sound basis for calculating accurate direct dielectronic recombination coefficients and ionisation coefficients even in static conditions.

In summary, for modelling and spectral analysis of the divertor, we prepare a number of types of derived datasets. These fall into two classes, namely those required to establish the distribution of impurity ions in the divertor. These data are used by the impurity transport models. Then there is the class of derived data required to interpret the radiation losses from the plasma. These include total radiated power at the grossed-up end of the scale and emissivities of specific lines at the other. Also, for quick inferences of impurity influx and emission shell shapes, one or two other forms of derived data are usually created. Such data can allow either reduction of the calibrated observed photon counts to physical quantities or can enter simulation of the spectrometer signals for matching with observation. These datasets are summarised in table

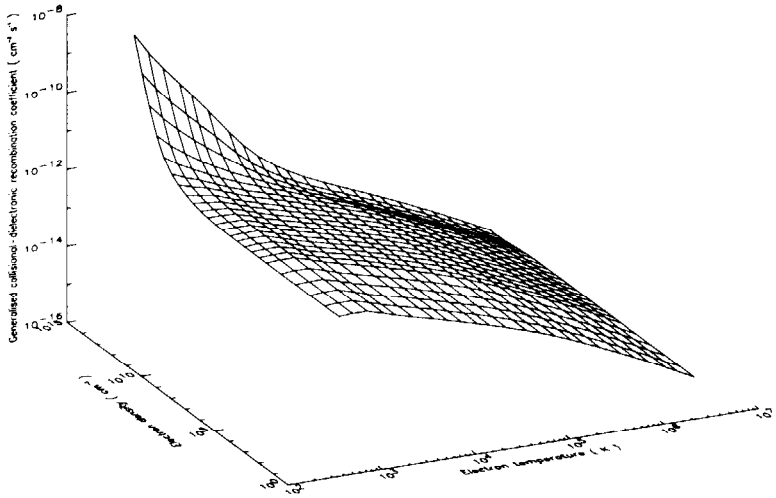

FIGURE 13. Generalised collisional-radiative recombination coefficient for $C^{+2}_{2s2p\ ^3P} + e \rightarrow C^{+1}_{2s^22p\ ^2P}$. This is the metastable to ground state part of the metastable resolved data. Note that for the metastable parent dielectronic recombination is suppressed through secondary autoionisation.

IV A.

The various derived data sets summarised above are each functions of plasma electron temperature and plasma electron density. Also they are metastable resolved. Thus the effective recombination coefficient for $C^{+2} \rightarrow C^{+1}$ has separate parts for $2s^2\ ^1S \rightarrow 2s^22p\ ^2P$, $2s2p\ ^3P \rightarrow 2s^22p\ ^2P$ and $2s2p\ ^3P \rightarrow 2s2p^2\ ^4P$. In our progressive refinement of this type of data, we have now moved to tabulations at the fairly dense grid of temperature and densities shown in figure 12 for the $2s^2\ ^1S \rightarrow 2s^22p\ ^2P$ effective recombination coefficient for $C^{+2} \rightarrow C^{+1}$. Note that in practice the tabulation of data for members of the same isoelectronic sequence is made at z-scaled temperatures and densities. In contrast, the $2s2p\ ^3P \rightarrow 2s^22p\ ^2P$ coefficient representing recombination from the C^{+2} metastable has quite a different character because of secondary autoionisation.

In fusion application, we have become accustomed to emission coefficients for spectral transitions of an ion being driven principally by electron impact excitation from the ground state of the ion. In the generalised collisional-radiative picture, we must also include separate driving from distinguished metastables of the ion. With the focus of recent years being principally on influx of ions under ionising conditions, the above was usually sufficient. However, the recombining plasmas which now matter indicate that we must include the effective emission coefficients driven from the metastables of the

TABLE 1. Definition of ADAS derived datasets used in divertor modelling

adf type	Subcode	Content
adf11	acd	generalised collisional-radiative recombination coefficient
adf11	scd	generalised collisional-radiative ionisation coefficient
adf11	ccd	generalised collisional-radiative CX recomb. coefficient
adf11	qcd	generalised collisional-radiative cross-coupling coefficient
adf11	xcd	generalised collisional-radiative parent cross-coupling coefficient
adf11	prb	generalised collisional-radiative recomb/bremss. power coefficient
adf11	plt	generalised collisional-radiative low-level line coefficient
adf11	prc	generalised collisional-radiative CX recom. power coefficient
adf11	pls	generalised collisional-radiative specific line power coefficient
adf11	met	generalised collisional-radiative metastable fractions
adf13	sxb	ionisation per photon coefficients
adf15	pec	photon emissivity coefficients

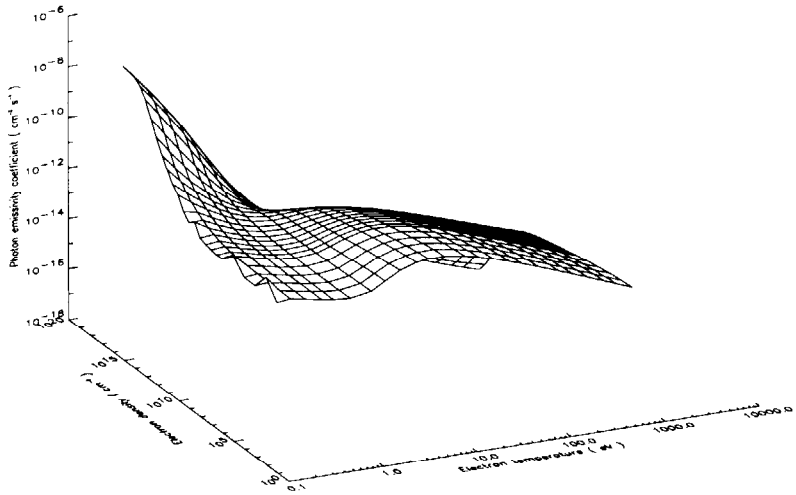

FIGURE 14. Generalised collisional-radiative emission coefficient for the $CII(2s^2 2p\ ^2P - 2s^2 3s\ ^2S)$ transition at 858.4Å. This coefficient is driven by recombination from the $C^{+2}_{2s^2\ 1S}$ state. Both direct radiative and dielectronic recombination as well as cascade are influential on populating this level at low density. At high density, the role of collisional-radiative redistribution is evident. The slight ripple at the lowest temperature is a numerical artifact.

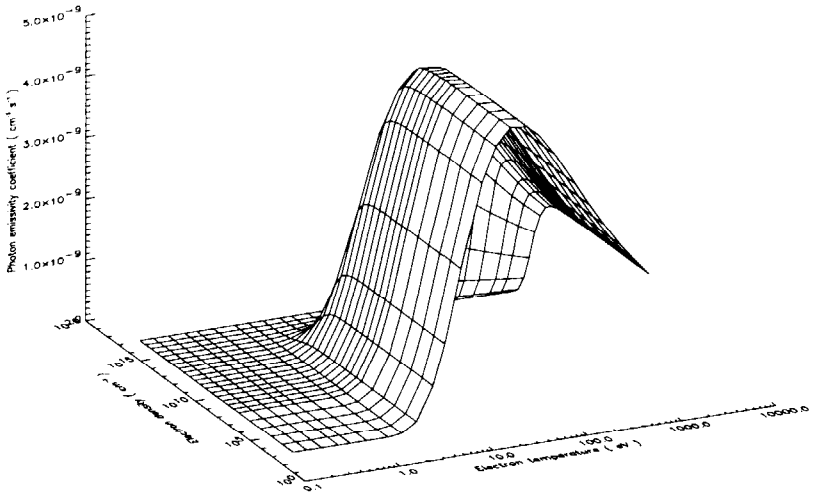

FIGURE 15. Generalised collisional-radiative emission coefficient for the $CII(2s^2 2p\ ^2P - 2s^2 3s\ ^2S)$ transition at 858.4Å. This coefficient is driven by excitation from the $C^{+1}_{2s^2 2p\ ^2P}$ ground state as evident from the exponential rise at low temperature. Note the suppression at high density as the collision limit moves down towards the upper level of the transition.

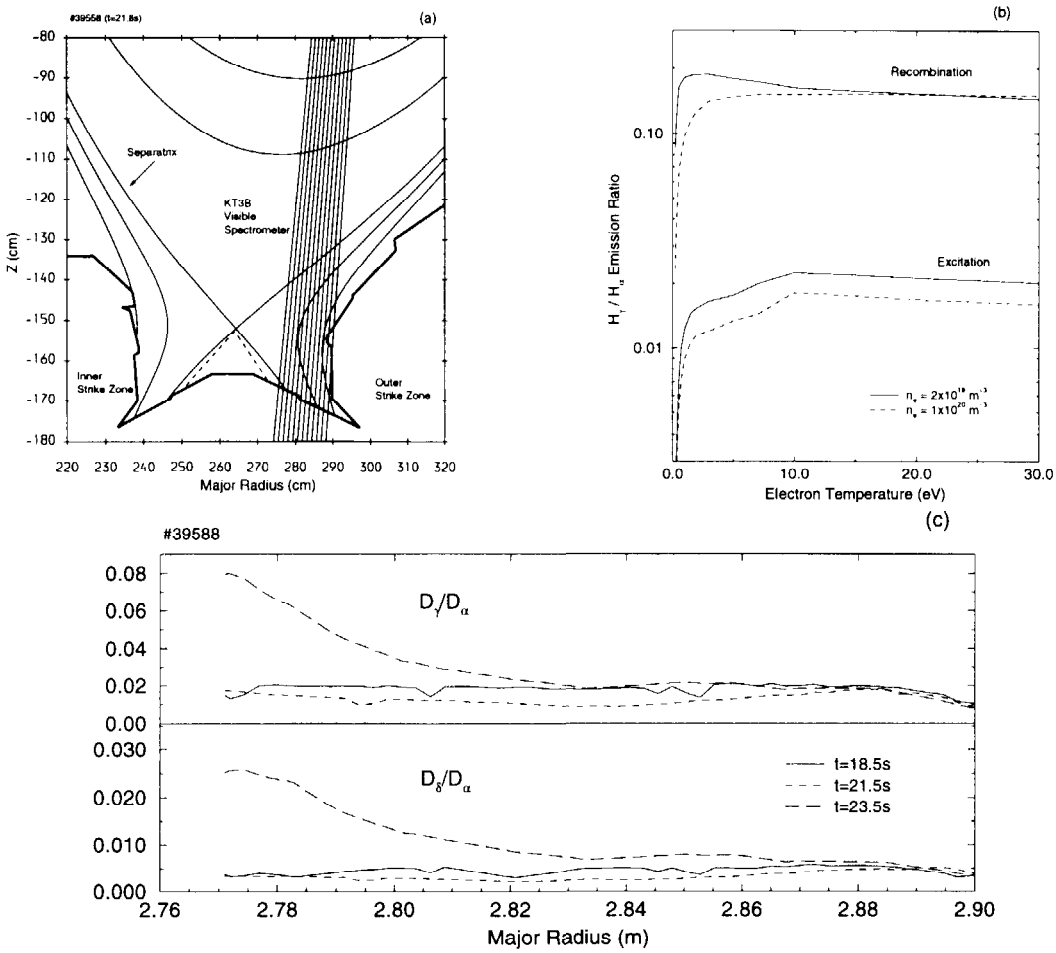

FIGURE 16. (a) Twelve lines of sight of the KT3B visible spectrometer directed at the outer divertor target; (b) Theoretical D_γ/D_α emissivity ratios drawn from the ADAS *adf*15 emissivity coefficient database; (c) Observed spatial variation of the D_γ/D_α and D_δ/D_α line ratios from the different KT3B lines of sight for JET discharge 39588 at times 18.5, 21.5 and 23.5 secs [D_α is a flux camera measurement]. From (c) at 18.5 sec., the D_γ/D_α ratio is ~ 0.02 over the range $R = 2.75 - 2.8$m consistent with an electron impact excitation mechanism for the lines at $N_e \sim 2 * 10^{19}\mathrm{m}^{-3}$. At 21.5 sec, all three line intensities have increased but D_α has peaked at ~ 2.80m resulting in a decrease of the D_γ/D_α and D_δ/D_α line ratios. This indicates a density increase but the line formation mechanism remains excitation. At 23.5 sec, D_γ/D_α changes markedly at small major radius - increasing to ~ 0.10. From (b), this is consistent with a change in line formation mechanism to recombination. Comparison with *adf*15 emissivity coefficients from ADAS indicates that both line ratios are consistent with $T_e = 0.7 - 0.9$ eV and $N_e \sim 2 * 10^{20}\mathrm{m}^{-3}$

next higher ion by recombination. These coefficients, formally present in generalised collisional-radiative modelling, were usually ignored previously except for less common lines emitted from higher n-shell states. Figure 14 shows the behaviour of this coefficient for a doublet line in the CII spectrum driven from the $2s^2\ ^1S$ ground of C^{+2} and is to be contrasted with figure 15 which is the coefficient for the same line, driven by electron impact from the C^{+1} ground state $2s^2 2p\ ^2P$. The divertor plasma at the time and point of detachment from the target is currently of interest and shows clear signatures of recombination. Figure 16 illustrates this in JET for deuterium itself. The analysis by McCracken draws upon collisional-radiative emissivity coefficients from the ADAS database.

V THE FUNDAMENTAL DATA

In this section, we wish to discuss briefly the steps involved in building collections of fundamental atomic data which are in some sense complete for the divertor application. In ADAS, these are called *adf*04 files. An *adf*04 file relates to a set of low levels of an ion - usually complete up to some n-shell - which spans the observational spectroscopy. The electron impact excitation part has been discussed on many occasions and again at this meeting. Here we wish to touch on the recombination part.

We seek to add free electron capture rate coefficients to each energy level of the set adopted for the ion. There are three parts to this, namely radiative recombination, dielectronic recombination and three-body recombination. The latter is the inverse of electron impact ionisation and enters at the collisional-radiative modelling stage. In a sophisticated formulation, radiative and dielectronic recombination occur as parts of one general process and can in principle interfere with each other. In practise, at least for light ions this is unimportant and radiative and dielectronic recombination can be treated as separate processes. Radiative recombination is obtained from the associated photo-ionisation cross-section via the Milne relation. If R-matrix photo-ionisation cross-sections [6] are used which include resonances then implicitly part of the dielectronic capture is added to the radiative recombination. This added part is not quite perfect since radiation damping of the resonances is not normally handled in R-matrix photo-ionisation cross-section calculations. However this is not a serious problem since regimes where the radiation damping matters can be isolated and treated separately as a dielectronic recombination calculation. Extended R-matrix photoionisation cross-section calculations have been carried out for astrophysics in the 'Opacity Project' [13]. Unfortunately, the only archived tabulations from these calculations do not resolve the final state of the photoionisation process! From the point-of-view of recombination, this means that the initial metastable from which recombination takes place is not identifiable. Thus the Opacity photoionisation data is not usable for our

present purpose. Some recomputation of Opacity R-matrix photo-ionisation cross-section data with resolution of final state and then preparation of state selective radiative recombination coefficients has taken place for Be-like ions $\rightarrow$ B-like ions at Queens's University, Belfast (Reid, 1997 - JET internal report). This has been contrasted with simpler one-electron, effective potential calculations using the observed quantum defects. In cases when dielectronic recombination can be ignored agreement is very good (error $\leq$ 20 %). It is our view that for fusion applications the latter method is mostly adequate. In ADAS, we archive state selective radiative recombination data in the data format *adf*08. This format is written to from the external refined calculation and also from an internal ADAS code operating the simpler approximation. Note that at moderate to high temperatures, the predominant part of the overall radiative recombinations takes place to resolved low levels spanned by our spectroscopic interest. At very low temperatures, the contributions to radiative recombination from capture to higher n-shells increase. Since purely hydrogenic rate coefficients are accurate to within a few per cent, the latter are used for high n-shells and generated internally in collisional-radiative codes.

Dielectronic recombination presents a more substantial problem. There are an abundance of dielectronic recombination results in the literature but these are virtually all summed over final (recombined) states and are only for recombination from the ground state of the recombining ion. Also, dielectronic recombination coefficients are required not only to low levels in a resolved picture but also to very many higher n-shells. These data must be archived unsummed so that the modifications of the effective recombination due to redistribution and reionisation can be evaluated properly. It must be stressed that zero-density dielectronic calculations of total effective recombination, even though accurately done, are quite inappropriate for light ions at the typical densities of divertor plasma. With such large data flows involved, we have found it a great advantage to interact directly with those able to generate such dielectronic data. This is so that a detailed prescription of the data layout can be agreed which fulfills the fusion need prior to substantive calculations. Within ADAS, this corresponds to another data format, *adf*09. Extensive state selective dielectronic recombination calculations, structured for ADAS were carried out in the period 1991-92 by Badnell (cf. Badnell, 1986 [2]). These data, for key light impurities of concern for fusion at that time, have now been substantial extended by O'Mullane and Badnell to cover all light ions up to neon. Nitrogen and neon have been of special importance in recent fusion experiments as impurities actively added to the plasma to enhance radiation emission in the divertor. Figure 17 gives some illustrative results for nitrogen. It is worth noting that the current fundamental dielectronic coefficients in ADAS occupy about 15 Mbytes. The *adf*08 and *adf*09 datasets provide the reservoir of state selective recombination data which are mapped onto the low levels of the *adf*04 datasets.

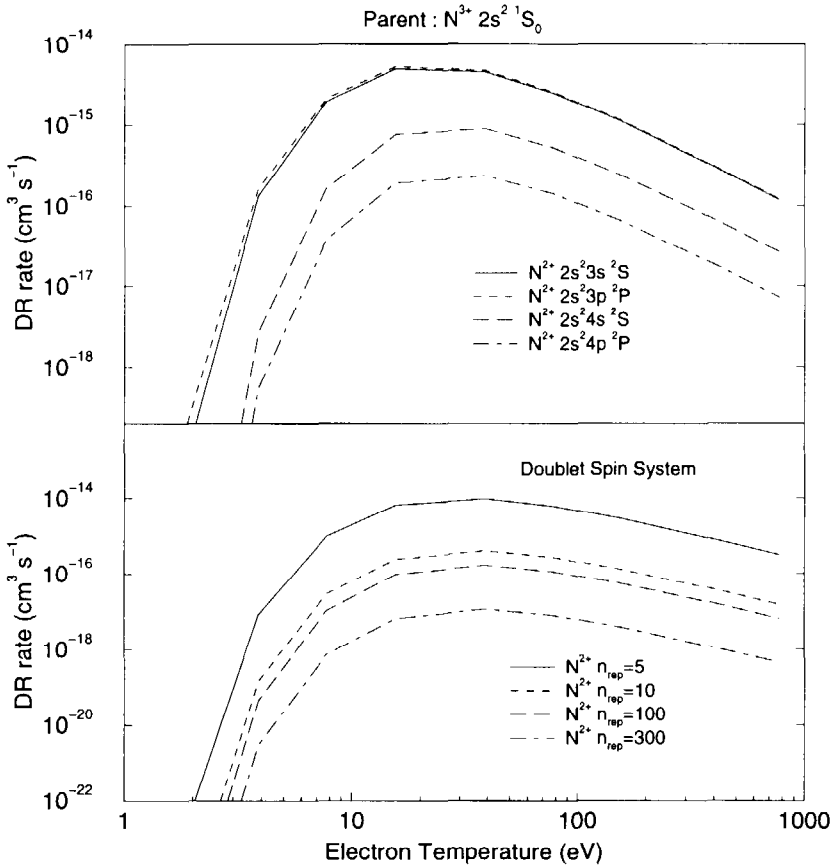

FIGURE 17. State selective dielectronic recombination coefficients to LS coupled terms and nS spin system shells of N^{+2} from the $N^{+3}_{2s^2\ ^1S}$ state occuring via $\Delta n = 0$ parent transitions. LS-resolved data is archived up to n=7. nS shell sums are archived for approximately 50 representative principal quantum numbers spanning from 2-1000. Note secondary auto-ionisation restricts the range of data built on metastable parents.

VI COLLISIONAL-RADIATIVE MODELLING AND THE COMPUTATIONAL IMPLEMENTATION

Clearly data sets of the *adf*04 type described above are the focus of all the highest quality data which can be mustered in support of analysis using the ion in question. As such they may reflect very considerable effort by many people. The datasets however remain incomplete for study of the populations in a plasma since they include only processes among the designated levels. From the point of view of recombination when dielectronic recombination is active, a very substantial downward cascade of electrons from higher n-shells occurs which markedly alters populations and indeed contributes the bulk of the effective recombination in the collisional-radiative sense. Conversely, for an ion in a low stage of ionisation in the relatively high densities and low temperatures of a divertor, populations of excited levels, for example in the $n = 3$ shell of N^{+2}, experience ionising collisions. Also this ionisation is not necessarily direct but may occur in a stepwise fashion through a series of higher excited n-shells. Finally even at low density, excitation from the ground level to higher n-shells followed by cascade gives a significant correction to that from direct excitation. The effects of higher n-shells must be included therefore to allow the precision obtainable in principle from the quality of the lower n-shell data. The estimation of the influence of higher n-shells may be calculated in simpler approximation since for such levels sub-shell mixing within an n-shell is very strong. At JET, we conduct such calculations within a parent and spin system resolved 'bundle-n' model and generate from it so-called 'condensed projection matrices'. These are archived in the database and need not change as refinement of the low level data proceeds with time. Thus for the complete treatment of an ion, collisional-radiative population codes draw both upon the detailed specific ion file of type *adf*04 in ADAS and also upon the projection matrices (called *adf*17 in ADAS). Together, these datasets and the subsequent population calculations allow us to realise all the derived collisional-radiative data actually used in analysis and modelling. For us, such datasets are the structures into which we seek to meld disparate fundamental data from many sources.

The above considerations indicate that our derived atomic calculations must be in the collisional-radiative framework. That is, as well as dealing with the mixture of collisional and radiative processes affecting population lifetimes, we must contrast atomic and plasma transport timescales. Collisional-radiative theory provides the prescription for separating populations into those which are short lived, reflecting local conditions only and those which are long-lived, reflecting their past history. The former are small populations (the true excited state populations) which can be treated as quasi-static yet provide the spectral emission, while the latter are large and must enter the plasma transport equa-

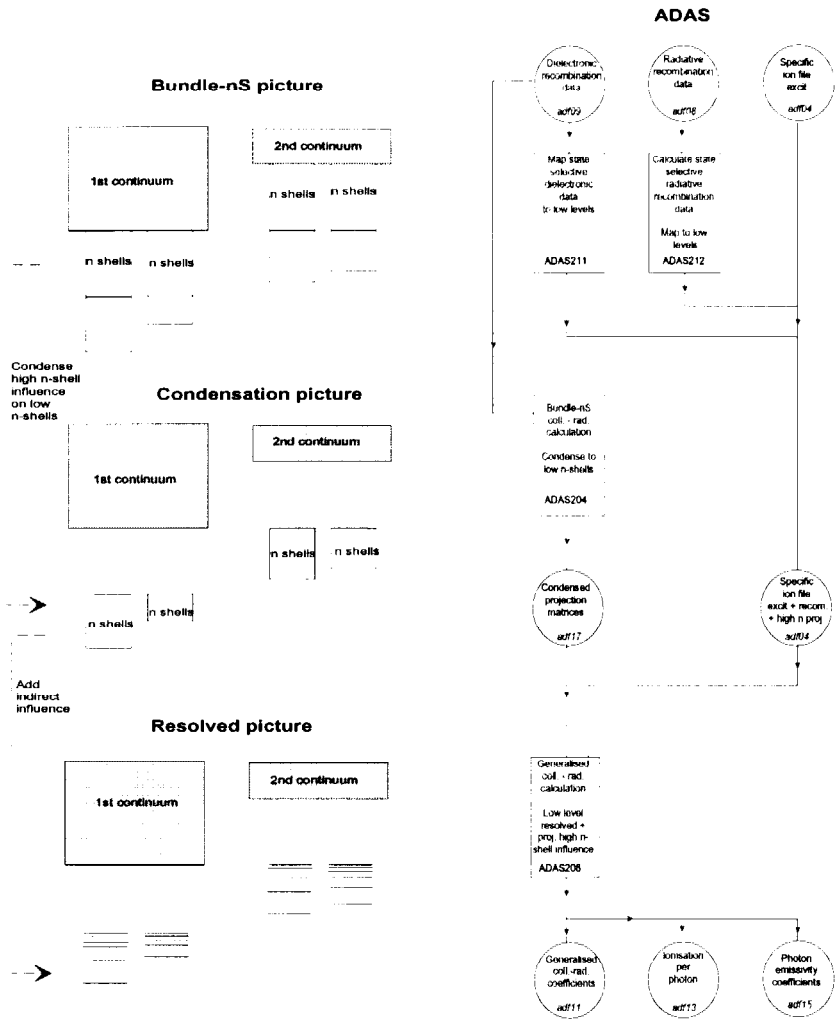

FIGURE 18. Schematic of mapping state-selective radiative and dielectronic recombination coefficients to specific ion files of type *adf*04 for low level resolved population calculations and to bundle-nS population models for the very many n-shell analysis. The lower section of the schematic shows the condensation of the results of the bundle-nS model onto low levels via condensed projection matrices (*adf*17) and then their mapping into the final high-level-influence-supplemented, resolved, low level, collisional-radiative calculation in which all the required metastable-resolved generalised derived data of table 1 are generated.

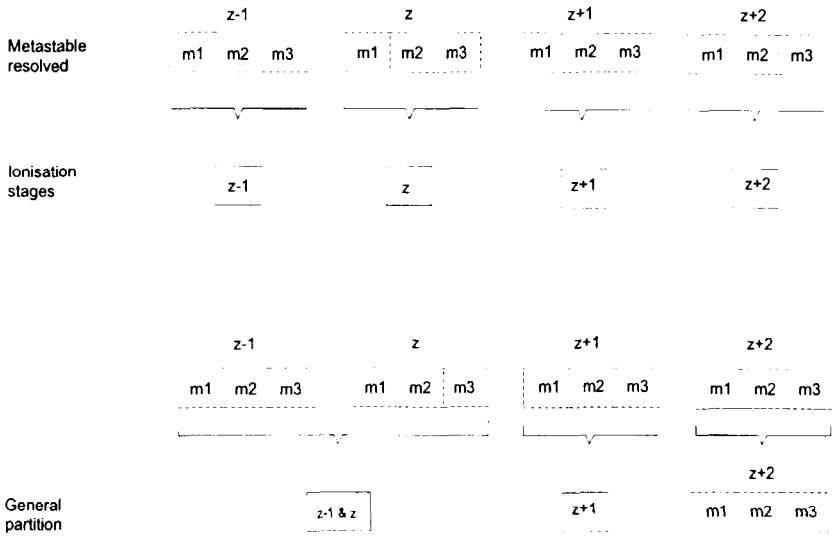

FIGURE 19. Schematic of flexible partitioning and condensing of metastable resolved collisional-radiative coefficient data as appropriate for the modelling and analysis.

tions explicitly. Generically, we call these large populations metastables. They include the ground populations of ionisation stages. Most plasma transport models, in fact, only include the ground state populations (or effectively the ionisation stage populations). The earlier illustrations in this paper indicate that the ground and low lying metastables are the 'correct' set of 'metastables' for a comprehensive picture. The production target of our collisional-radiative atomic modelling should be derived data relative to the complete set of metastables in the first instance, although it is perfectly reasonable to simplify further later according to more specific conditions or available resources. From a practical point of view, the collisional radiative separation (we use the name 'generalised collisional-radiative' when we include the complete set of metastables) provides effective ionisation coefficients, effective recombination coefficients etc. which link metastable population to metastable population and then effective emission coefficients which give the spectral emission possible from the quasi-static populations once the metastable populations are known. Figure 18 illustrates the implementation of these ideas in ADAS as used for JET divertor modelling and analysis.

VII DISCUSSION AND CONCLUSIONS

The level of complexity involved in metastable resolution certainly matters for ionisation stages which are targetted for spectroscopic diagnostic use, but may be excessive for less important ionisation stages and simpler modelling. This is especially true for heavy species with many ionisation stages.

To allow practical computations with reasonable execution times and storage requirements, it is helpful to reduce the effective number of populations (stages, grounds or metastables) to be handled. We have found it useful to arrange our primary storage of metastable resolved collisional-radiative data by isoelectronic sequence as indicated above. A separate computational step then gathers together those ions from the iso-electronic sequence archives to assemble an iso-nuclear sequence (that is the data for a particular element). This gathering step can simultaneously implement a condensation of the data in a manner tuned to the intended use. A schematic is shown in figure 19. We define a partition of the complete list of metastable states which specifies a grouping. The metastable resolved equilibrium ionisation balance can be used to decide the proportions to be used in generating a new condensed set of collisional-radiative data linking partition member to partition member. The simplest condensing partition is to combine metastables belonging to the same ionisation stage. Such a condensation restores the usual stage to stage data but with a sounder pedigree. At JET for light ions we have worked mostly with the fully metastable resolved partition and the stage partition.

It is satisfying to observe in the illustrations given here and studies elsewhere that extensive and sophisticated fundamental atomic data are being brought into play in analysis of fusion plasma diagnostic measurements. However, this does require exploitation of the collisional-radiative method, a structured approach to fundamental data and the provision of appropriate derived data at the point of analysis. At JET, we have found that ADAS has helped in these matters. Through its shared use and development with associated laboratories operating different machines, it has strengthened interpretation.

REFERENCES

1. Anderson, H. *in preparation* (1997).
2. Badnell N. R. *J. Phys. B* **19**, 3827 (1986).
3. Bliek F. W., Hoekstra R., Olson R. E. et al. *J. Phys. B* - in preparation (1997)
4. Boileau A., von Hellermann M., Mandl W. et al. 1989 *J. Phys. B* **22**, L145 (1989).
5. Breger P. and Vlases G. *JET Joint Undertaking Report* JET-TN(91)04 (1991).
6. Burke P. G. and Berrington K. A. *Atomic and Molecular Processes: An R-matrix Approach* (IOP Publishing Ltd.) (1993).
7. Duxbury G., Summers H. P. and Stamp M. *JET Joint Undertaking Report*, JET-P(97)18 (1997).
8. Griffin D. C., Pindzola M. S., Shaw J. A., Badnell N. R., Summers H. .P and O'Mullane M. *J. Phys. B* **30**, 3543 (1997).
9. von Hellermann M. *Atomic and Plasma-Material Interaction Processes in Controlled Thermonuclear Fusion* - ed. R K Janev and H W Drawin, p135 (Elsevier, Amsterdam) (1993).
10. Hoekstra R., et al. *these proceedings* (1997).

11. Maggi C. F. M. *Ph.D. Thesis* University of Strathclyde (1997).
12. Maggi C. F., Elder J. D., Fundamenski W. et al. *J. Nucl. Mat.* **241-243**, 414 (1997).
13. Seaton M .J. *J. Phys. B* **20**, 6363 (1987).
14. Summers H. P. *Adv. At. Mol. and Opt. Physics* **33**, 275 (1994).
15. Summers H. P. *Atomic Data and Analysis Structure* JET Joint (1994). Undertaking Report JET-IR(94)06; *http : //patiala.phys.strath.ac.uk/adas/*
16. Summers H. P. and Dickson W. *Recombination of Atomic Ions* - ed. W G Graham, p31 (Plenum, New York) (1992).